Grapevine Shiraz Disease-associated viruses lead to significant yield losses by altering transcription of genes related to defence responses and photosynthesis

Dilrukshi S. K. Nagahatenna[1*], Cristobal Onetto[1,2*], Yeniu Mickey Wang[1,3], Anthony Borneman[1,2], Vinay Pagay[1†]

[1]School of Agriculture, Food and Wine, Waite Research Institute, The University of Adelaide, PMB 1, Glen Osmond, SA, Australia 5064.

[2]The Australian Wine Research Institute, Glen Osmond, SA, Australia 5064.

[3]CSIRO, Manufacturing, Autonomous Sensors Future Science Platform, 13 Kintore Ave, Adelaide, SA, Australia 5000.

[*]Authors contributed equally

[†]Corresponding Author

e-mail: vinay.pagay@adelaide.edu.au

Abstract

Grapevine Shiraz disease (SD), which is associated with Grapevine Virus A (GVA), is one of the highly destructive diseases affecting Australian and South African vineyards. However, virtually nothing is known about the transcriptional modifications in grapevine phloem tissues induced by SD as well as its impact on vine physiology, yield and fruit composition. In this study, we assessed the physiological parameters of SD-infected *Vitis vinifera* L. cv. Shiraz vines grown in a commercial vineyard in South Australia over two growing seasons. Viruses present in symptomatic SD-affected and asymptomatic vines were investigated using serological (ELISA) and molecular tests (PCR and Illumina next generation sequencing). SD did not alter plant water status over the growing season, however significantly decreased canopy size, leaf gas exchange, chlorophyll fluorescence, and yield. Differential gene expression analysis revealed significantly higher expression of genes associated with systemic acquired resistance (SAR) and downregulation of defence- and photosynthesis-related genes in phloem tissues of SD vines. This is the first comprehensive report of the physiological and transcriptomic responses of grapevine to SD.

Key words: Grapevine Virus A, Grapevine leafroll virus, Systemic Acquired Resistance, Transcriptomics, ELISA

Introduction

Grapevine (*Vitis vinifera* L.) is a major perennial horticultural crop grown in diverse climatic regions around the world. As grapevine is vegetatively propagated, it is highly susceptible to graft- and vector-transmitted pathogens. Currently, approximately 86 phloem-limited viruses have been reported in grapevine [1]. Among them a *Vitivirus*, Grapevine Virus A (GVA), which belongs to the family *Betaflexiviridae* [2], is considered to be the primary causal agent associated with highly destructive Shiraz Disease (SD) [3]. This disease has been

reported only in South Africa and Australia, and previous studies have demonstrated that SD symptoms are prominent in susceptible cultivars infected with either GVA alone, or as a co-infection with variants of grapevine leafroll associated virus (GLRaV), including GLRaV-1, GLRaV-3, or GLRaV-4 strain 9 [3-5]. Both GVA and GLRaV are phloem-limited and are generally transmitted either by grafting or insect pests such as mealybugs and scale insects [6, 7]. The grapevine cultivars Shiraz, Merlot, Gamay, Malbec and Viognier are highly susceptible to SD [8], with infected vines displaying primary bud necrosis, retarded shoot growth and delayed senescence of crimson-coloured leaves [3]. However, other infected cultivars such as Cabernet Sauvignon do not exhibit any of the SD-symptoms mentioned above [9].

The genome of GVA comprises a 7349-7351 nucleotide-long positive-sense stranded RNA (excluding a poly(A) tail at the 3' terminus) that is arranged into five open reading frames (ORF1-5) [10, 11]. Biological and molecular studies in *Nicotiana benthamiana* revealed that GVA possesses extensive genetic heterogeneity [3, 8, 12, 13] and their variants have been classified into three molecular groups based on nucleotide similarity [14]. Variants of molecular groups I and III are often asymptomatic whereas variants of group II are found to be closely associated with SD and often symptomatic [3, 4, 13, 14].

To date, studies into SD have largely focused on understanding GVA genomic sequence differences and developing molecular diagnostic techniques to reliably detect disease infections in the vineyard. Even though GVA is one of the most frequently detected phloem-borne viruses in Australian vineyards, virtually no comprehensive studies have been conducted to elucidate the pathogenicity of the virus and impacts of SD on vine physiology, yield and fruit composition. Our understanding of the mechanisms by which phloem-borne grapevine pathogens exploit phloem tissues are scarce because of the difficulty in studying phloem tissue-specific processes. While, previous studies have revealed a sequence similarity between South African and Australian GVA variants [3, 14], SD-infected vines in Australian vineyards do not express the severe vine mortality symptoms that are commonly observed in SD-infected vines in South Africa. Therefore, the main objectives of this study were to apply high-throughput sequencing to investigate both RNA-based viral content as well as SD-induced transcriptomic changes in the phloem tissues of grapevines, and to correlate this data with physiological and agronomic impacts observed in the grapevines and vineyards.

Materials and Methods

Experimental site

The study was conducted over two growing seasons (2020/2021 and 2021/2022) in a commercial vineyard located in Riverland, South Australia. *Vitis vinifera* L. cv. Shiraz vines included in the study were grafted onto K51-40 rootstock and planted in 1998 with a spacing of 3.5 m and 3.5 m within and between rows, respectively, and oriented E-W direction. The vines were drip-irrigated and fertilised according to the standard practices for the region. Vines were spur pruned and shoots produced from bilateral cordons were trained to vertical shoot positioning (VSP). Weather data was collected from an automatic weather station maintained by the Australian Bureau of Meteorology (Station ID: 024048) located in Renmark, SA, approx. 11 km from the vineyard.

Identification of viral diversity in asymptomatic and Shiraz diseased vines

Over the course of both growing seasons, all vines were visually assessed for SD symptoms. Depending on the severity of the symptoms at the harvest stage (in March), cane samples of pencil thickness (diameter approx. 7 mm) were collected from 32 vines and tested by commercial Enzyme-linked Immunosorbent Assay (ELISA) kits (Bioreba, Switzerland) for the presence of GLRaV-1, GLRaV-3, GLRaV-4s and GVA according to the manufacturer's instructions. A subset of cane samples was sent to a commercial diagnostics laboratory (Affinity Labs, Adelaide, Australia) for confirmation by multiplex RT-PCR using primers specific to GLRaV-1, GLRaV-3, GLRaV-4s (strains 4, 6 and 9) and GVA.

In the second season (2021/2022), viral diversity and abundance were evaluated using Illumina next generation sequencing in several asymptomatic and SD-infected vines.

Physiological measurements

Grapevine physiological performance was evaluated in 20 vines, 10 asymptomatic and 10 SD-infected, at three phenological stages – fruit set, veraison and harvest – over both growing seasons. Canopy size was estimated via leaf area index (LAI) measurements using a ceptometer (Model: Accupar LP-80, Meter Group, Pullman, WA, USA). Midday stem water potential was measured on one fully-expanded (mature) leaf per vine using a Scholander-type pressure chamber (Model 1505, PMS Instruments, Albany, NY USA) as described in Pagay [15].

In vivo leaf gas exchange was measured using a portable infrared gas analyser (Model: LI-6400XT, LI-COR Inc., Lincoln, NE, USA) as described in Pagay [15]. Chlorophyll fluorescence parameters were measured with a LI-6400XT equipped with a leaf chamber fluorometer (Model: 6400-40, LI-COR Inc., Lincoln, NE, USA) in dark- and light-adapted fully expanded leaves positioned in the bottom, middle and top parts of the shoot of each vine. In light-adapted leaves, the steady-state fluorescence yield (F_s) was measured. Then, a saturating white light pulse (8,000 μmol m^{-2} s^{-1}) was applied for 0.8 s to achieve the light-adapted maximum fluorescence (F_m'). The actinic light was then turned off, and far-red illumination was applied (2 μmol m^{-2} s^{-1}) to measure the light-adapted initial fluorescence (F_0'). Dark-adapted measures were performed by covering the leaves with dark-adapting leaf clips (Model: 9964-091, LI-COR Inc., Lincoln, NE, USA) for at least 30 min prior to measurement. Basal fluorescence (F_0) and maximum fluorescence emission (F_m) were measured by illuminating leaves to a weak modulating beam at 0.03 μmol m^{-2} s^{-1} and saturating white light pulses of 8,000 μmol m^{-2} s^{-1}, respectively. Photochemical quenching coefficient (qP) and actual photochemical efficiency of PSII (Φ_{PSII}) were calculated as: $qP = (F_m' - F_s)/(F_m' - F_0')$ [16], $\Phi_{PSII} = (F_m' - F_s)/F_m'$ [16]. Electron transport rate (ETR) was calculated according to Rahimzadeh-Bajgiran, Tubuxin [17] using the following equation:

$$ETR = \Delta F/F_m' \times PPFD \times 0.5 \times 0.875$$

where, $\Delta F/F_m'$ is the PSII photochemical efficiency (Φ_{PSII}), PPFD is the photosynthetic photon flux density incident on the leaf, 0.5 is a factor that assumes equal distribution of energy between the two photosystems, and 0.875 is the assumed leaf absorptance [18, 19]. Mesophyll conductance (g_m) was calculated using a theoretical value of non-respiratory CO_2 compensation point Γ^*=42.9 μmol mol^{-1} (ppm) CO_2 [20].

RNA extraction and sequencing

In order to capture viral genomic sequences and investigate SD-induced differentially expressed transcriptomic changes, eight asymptomatic and four SD vines were selected. Lignified canes (diameter approx. 7 mm) were collected from cordon spur positions of each vine following harvest of the 2020/2021 season. The bark was immediately removed with a sharp blade, the phloem tissues were collected and cut into small pieces. The samples were stored in liquid nitrogen in the field, transported to the laboratory at the University of Adelaide (Waite Campus) where they were transferred to a -80 °C freezer until further analysis.

RNA was extracted from approximately 100 mg of frozen samples according to a modified RNeasy Plant Mini Kit (Qiagen, Germany) procedure [21]. Samples were homogenized with 1 mL of RLT lysis buffer supplemented with 2.5% (w/v) polyvinylpyrrolidone-40 (PVP-40) and 1% (v/v) *β*-mercaptoethanol (*β* -ME). After vortexing, the homogenate was mixed with 1/10 volume of 20% (v/v) *N*-lauroylsarcosine (Sigma-Aldrich, Australia) and incubated at 70 °C for 10 min. Samples were centrifuged at 13,000 rpm for 5 min and approx. 700 μL of the supernatant was transferred to a QIAshredder column. Contaminated DNA was removed according to On-column DNase digestion protocol (Sigma, USA). The amount of total RNA was quantified using a Qubit fluorometer. Plant ribosomal RNA were depleted using QIAseq FastSelect rRNA Plant Kit (Qiagen, Australia) as described in Liefting, Waite [22]. Library preparation and sequencing was performed in the Ramaciotti Centre for Genomics (University of New South Wales, Sydney, Australia). Sequencing libraries were prepared using the Illumina stranded mRNA kit and sequenced with an Illumina NovaSeq 6000 using 2 x 150 bp chemistry on a S4 flow cell.

Sequence assembly and RNA virus discovery

Illumina paired-end reads were quality trimmed and rRNA depleted using fastp v. 0.23.2 (Chen et al., 2018) and RiboDetector v. 0.2.7 [23], respectively. Initial transcriptome assembly was performed using Trinity v. 2.8.5 [24]. Taxonomic classification of assembled contigs was performed using Kaiju v. 1.9.0 against the nr-euk database. Contigs larger than 3 kb and taxonomically classified as belonging to the Virus superkingdom were retained and queried (blastn) against the GenBank nr nucleotide database for taxonomic assignment. Illumina reads were then mapped back to the transcriptome assembly using Bowtie v. 1.3.1 [25] and the relative abundance of individual contigs were estimated using the RNA-Seq by Expectation Maximization (RSEM) algorithm implemented within Trinity [26]. For phylogenetic analysis, near-complete virus genomes were direction adjusted and aligned using MAFFT v 7.487 [27]. Maximum likelihood phylogenetic reconstruction was performed using IQ-TREE v. 2.1.2 [28] and the best substitution model automatically selected using ModelFinder [29].

Differential transcript expression analysis

Quality trimmed and rRNA depleted paired-end RNA-Seq reads were used to quantify transcript abundance in grapevine using annotated CDS sequences of the *Vitis vinifera* 12X Ensembl reference genome (PN40024.v4) and Kallisto v. 0.48 [30]. Read count tables were imported into R, features with 0 counts in all samples and a total count < 10 were removed, and differential expression analysis was performed using the DESeq2 package v.1.24.0 [31] with default parameters (sample-wise size factor normalization, Cox-Reid dispersion estimate and the Wald test for differential expression) and shrunken Log2 fold-changes. Features with a Log2 fold-change (Log2FC) of 1 < Log2FC < -1 and an adjusted p-value < 0.005 were considered for further analysis. Gene

ontology enrichment analysis of the ordered differentially expressed transcripts was performed using g:Profiler [32].

Yield components

In line with the commercial harvest, grape bunches were harvested in early March during both seasons. Total yield, total bunch count and 50 berry weight were recorded for each vine and used to calculate yield components including yield per m, bunch count per m, average berry weight, average bunch weight and berries per bunch.

Fruit chemical composition

Fruit samples were stored at 4 °C after harvest and total soluble solids (TSS) was measured within 2-3 days after berries were returned to room temperature using a refractometer (Model: PAL-BX|ACID2, Atago, Tokyo, Japan). Juice was extracted from 200 g of berries from each vine using a fruit juicer (Russell Hobbs Model: RHSJ100, Spectrum Brands, Braeside, VIC, Australia). Juice pH and titratable acidity (TA) were simultaneously assessed using an autotitrator (Model: T50, Mettler Toledo, Columbus, OH, USA). Grape juice colour and hue were calculated using absorbance at 420 nm and 520 nm respectively, using a solution of 20% glucose and 1 g tartaric acid as a blank. Colour density and hue/tint were calculated using the following formula: Colour density = $A_{520} + A_{420}$, Hue/Tint = A_{420}/A_{520}.

Total anthocyanin content was determined using a pH shift method. Ten-fold diluted samples were prepared using pH 1.0 and pH 4.5 buffers, and absorbance at 520 nm was measured following 1 h of dark incubation. Total anthocyanin concentration was calculated as malvidin chloride 3, 5-diglucoside equivalents using the following formula:

$$\text{Total anthocyanins (mg/L)} = (A^{520}_{\text{pH 1.0}} - A^{520}_{\text{pH 4.5}}) \times 255.75$$

For the total phenolics assay, 2 uL of the sample (or 20 µL of the 10:1 diluted sample), 1.58 mL of distilled water and 100 µL of Folin & Ciocalteu phenol reagent were added to a glass cuvette, and after 1 min incubation at room temperature, 300 µL of sodium carbonate solution was added. The solution was incubated at 40 °C for 30 min under dark and absorbance was measured at 765 nm against a blank. Total phenolics were then quantified using a Gallic acid standard curve and expressed in mg/L of gallic acid equivalents (GAE).

Leaf nutrient analysis

Approximately five mature green leaves were collected from random locations in each vine, and samples were sent to a commercial plant nutrient testing lab (APAL, Adelaide, Australia) for leaf nutrient analyses.

Statistical analysis

Statistical analysis was carried out using Prism software (version 9.0.0, GraphPad Software, San Diego, CA). Unpaired t-tests were used to assess differences between treatments in the first season, and one-way ANOVA was used for the second season. Two-way ANOVA was used for analysis that involved two or more factors and Tukey multiple comparisons posthoc test ($\alpha = 0.05$) was applied for multiple groups. Non-linear regressions were used to assess differences between each soil type and means were tested using the sum-of-squares F test to evaluate whether slopes were significantly different ($P < 0.05$).

Sequencing data availability

The sequencing data and viral assembled contigs included in this study are publicly available at NCBI under Bioproject PRJNA1085026.

Results

Abundance of RNA viruses in asymptomatic and SD vines

During our preliminary study, all 32 of the pre-selected vines were analysed for SD-associated viruses using serological and multiplex RT-PCR. Nineteen asymptomatic vines were found to be negative for GVA, GLRaV-1, GLRaV-3 and GLRaV-4s, whereas 13 SD vines tested positive for GVA and GLRaV-4s (strain 9). Viral diversity was further investigated in twelve samples by *de novo* assembling of sequencing data and comparing viral contigs to known grapevine virus genomes.

Illumina sequencing allowed for the identification of near-complete genomes of five viral species corresponding to four genera (*Ampelovirus*, *Foveavirus*, *Marafivirus* and *Vitivirus*) of positive-sense ssRNA viruses that had been previously reported in grapevine [33] (Figure 1a). In agreement with the ELISA and RT-PCR tests, genomes of GVA and GLRaV-4 were found in SD-symptomatic samples only. Additionally, genomes matching grapevine rupestris stem pitting-associated virus (GRSPaV) and grapevine rupestris vein feathering virus (GRVFV) were also observed in all symptomatic vines (Figure 1a). No viral contigs taxonomically classified as GVA or GLRaV-4 were recovered from asymptomatic samples, however, the species GRSPaV was observed in all samples, and GRVFV in six out of the eight asymptomatic samples investigated (Figure 1a). Fragmented contigs corresponding to Grapevine Syrah virus 1 (GSyV-1) were recovered in three asymptomatic samples (7-9, 14-6, 23-18) (Figure 1a).

Virus relative abundance was estimated from the proportion of the total viral reads in each library after removal of rRNA reads. Relative abundance of two housekeeping genes was also estimated, indicating a homogenous host sequencing depth across all samples (Figure 1b). There were large differences in viral abundance between samples, with SD symptomatic vines displaying more than two-fold increase in total viral abundance relative to asymptomatic vines (Figure 1a). Within SD vines, sample 7-16 displayed the highest total viral abundance as well as the highest abundance of GVA and GLRaV-4 (Figure 1a).

Maximum likelihood phylogenetic reconstruction for GVA and GLRaV-4 was performed using publicly available genomes for GVA (Figure 1c) and grapevine leafroll-associated members of the genus *Ampelovirus* (Figure 1d). Inspection of tree topology confirmed the presence of GVA group II (Figure 1c) and GLRaV-4 strain 9 (Figure 1d) in all SD vines. Samples 14-11, 7-16 and 7-13 also contained viral contigs corresponding to GVA group III (Figure 1c).

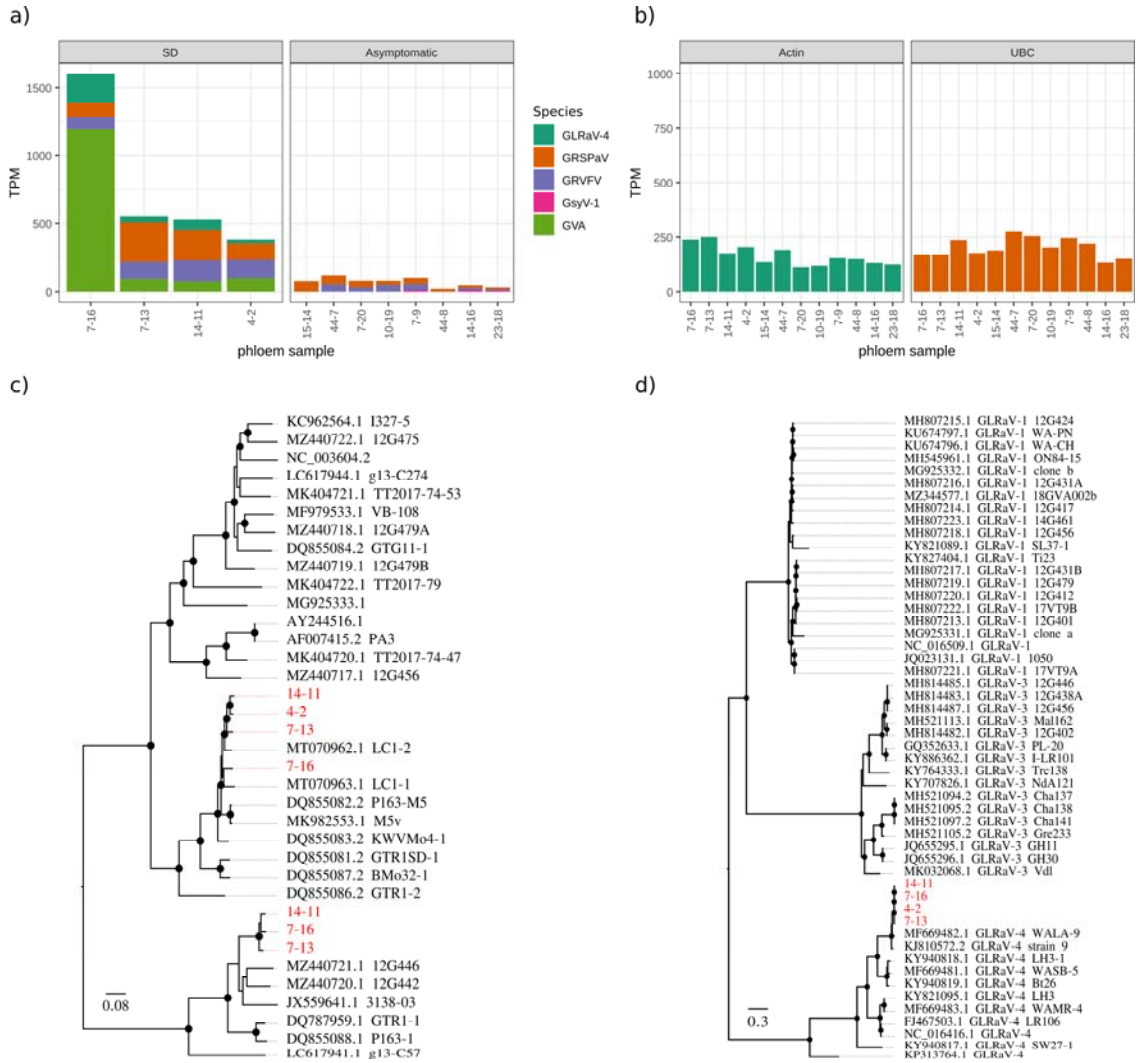

Figure 1. Diversity and abundance of RNA viruses in 12 phloem tissue samples. Transcript relative abundance (TPM, transcripts per million transcripts) of viral contigs (a) and two housekeeping genes (b) in samples obtained from asymptomatic and Shiraz Disease (SD) symptomatic grapevines. Maximum likelihood unrooted phylogenetic tree predicted from the sequence alignment of near-complete (c) GVA and (d) *Ampelovirus* grapevine leafroll genomes available at NCBI. Viral genomes assembled in this study are coloured in red. Black circled nodes represent a bootstrap support > 90%.

Physiological performance of asymptomatic and SD vines

Bud burst was significantly delayed in SD vines compared to healthy vines (data not shown). The delayed bud burst resulted in leaf area index (LAI) values that were considerably lower in the SD vines at the beginning of both seasons (data not shown). By the end of the season, close to harvest, no significant differences in LAI were observed between SD-infected and healthy vines (Table 1). SD vines also had similar plant water status (Ψ_{stem}) compared to healthy vines; the values across both groups reflected good vine water status. Leaf gas exchange was consistently lower in the diseased vines in both seasons of this study. There were drastic (up to 50%) reductions in leaf net photosynthesis and stomatal conductance in the diseased vines (compared to the healthy

vines), while the intrinsic water use efficiency (WUE_i) increased up to 40% in the diseased vines. Leaf chlorophyll fluorescence parameters, as measured with a fluorometer, indicated that dark-adapted leaves had similar maximum quantum efficiency of photosystem II (PSII), F_v/F_m, but the light-adapted leaves had lower values of F_v'/F_m' when diseased, particularly in Season 2 (2021/22). This trend was also observed for the other fluorescence parameters including Φ_{PSII} and *ETR*. It seems evident that cumulative stresses resulting from SD infections results in lower physiological performance at the leaf-level as indicated in the data from the second season. Photochemical quenching (*qP*) was higher in the healthy vines during the second season.

Table 1. Grapevine physiological performance of Shiraz Disease (SD)-infected and SD-free (healthy) vines at the pre-harvest stage (E-L37) of grapevine development in the 2020/21 and 2021/22 seasons (n=10).

Parameter	**2020/21**			**2021/22**		
	SD-free	**SD-infected**	***P*-value**	**SD-free**	**SD-infected**	***P*-value**
Canopy Size						
LAI	10.6 ± 0.23	10.1 ± 0.32	0.3345	9.18 ± 0.31	8.46 ± 0.51	0.1546
Vine Water Status						
Ψ_{stem}	-0.51 ± 0.01	-0.51 ± 0.02	0.9050	-0.49 ± 0.02	-0.48 ± 0.01	0.8376
Leaf Gas Exchange						
A_n	11.2 ± 1.0	7.8 ± 0.8	0.0224	13.2 ± 0.8	6.8 ± 0.9	< 0.0001
g_s	0.123 ± 0.01	0.071 ± 0.02	0.0180	0.183 ± 0.02	0.094 ± 0.02	0.0071
c_i	214 ± 10	183 ± 19	0.1536	248 ± 6	235 ± 10	0.2875
E	3.81 ± 0.36	2.31 ± 0.39	0.0108	6.56 ± 0.47	3.77 ± 0.64	0.0029
WUE_i	93.1 ± 6.1	129.3 ± 17.0	0.0601	74.9 ± 3.7	84.9 ± 6.4	0.2075
Leaf Chlorophyll Fluorescence						
F_v/F_m	0.76 ± 0.01	0.78 ± 0.01	0.2206	0.81 ± 0.00	0.80 ± 0.01	0.0967
F_v'/F_m'	0.43 ± 0.00	0.44 ± 0.06	0.8760	0.45 ± 0.01	0.36 ± 0.01	< 0.0001
Φ_{PSII}	0.20 ± 0.02	0.19 ± 0.01	0.6167	0.27 ± 0.02	0.17 ± 0.02	0.0006
ETR	132 ± 13	123 ± 9	0.5974	178 ± 12	110 ± 1	0.0006
qP	0.46 ± 0.04	0.46 ± 0.04	0.9041	0.60 ± 0.03	0.46 ± 0.03	0.0070

LAI = Leaf Area Index (m^2 m^{-2}); T = canopy porosity (%); Ψ_s = midday stem water potential (MPa); A_n = leaf net photosynthesis (μmol CO_2 m^{-2} s^{-1}); g_s = leaf stomatal conductance (mol H_2O m^{-2} s^{-1}); E = leaf transpiration rate (mmol H_2O m^{-2} s^{-1}); c_i = leaf intercellular CO_2 concentration (ppm); WUE_i = leaf intrinsic water use efficiency (μmol CO_2 / mol H_2O); F_v/F_m = maximum quantum efficiency of PSII, dark-adapted; F_v'/F_m' = maximum quantum efficiency of PSII, light-adapted; Φ_{PSII} = quantum yield of PSII; *ETR* = electron transport rate; *qP* = photochemical quenching.

Reproductive performance and fruit composition

Shiraz grapevines infected with SD had lower bunch numbers relative to healthy vines in both seasons (Table 2). Compared to the infected vines, there was a trend towards lower yields in the infected vines, likely attributable to the lower bunch numbers. Relative to healthy vines, the SD vines also had lower average bunch weights in the first season. Other yield components including berry weight were not impacted by SD.

Table 2. Yield components and fruit composition of SD and asymptomatic Shiraz grapevines over two seasons. Data are means ± SEM of 10 biological replicates for each healthy and SD groups.

Parameter	**2020/21**			**2021/22**		
	SD-free	**SD-infected**	***P*-value**	**SD-free**	**SD-infected**	***P*-value**
Yield (kg m^{-1})	14.8 ± 1.0	4.1 ± 0.5	0.1446	10.8 ± 0.8	1.8 ± 0.4	0.8887
Bunch count	133 ± 9	44 ± 5	<0.0001	93 ± 3	16 ± 4	<0.0001
Average bunch weight (g)	111.6 ± 3.7	91.9 ± 4.7	0.0001	116.3 ± 6.7	130.7 ± 15.6	0.4345
Average berry weight (g)	1.30 ± 0.03	1.20 ± 0.05	>0.9999	1.66 ± 0.04	1.68 ± 0.03	>0.9999
Total Soluble Solids (° Brix)	24.2 ± 0.8	24.0 ± 0.4	>0.9999	23.6 ± 0.4	24.5 ± 0.5	>0.9999
Titratable acidity (g L^{-1})	4.50 ± 0.16	5.40 ± 0.26	>0.9999	3.50 ± 0.16	3.90 ± 0.11	>0.9999
pH	3.66 ± 0.04	3.75 ± 0.02	>0.9999	4.01 ± 0.03	3.90 ± 0.05	>0.9999
Total Anthocyanins (mg L^{-1})	30.6 ± 1.7	46.5 ± 3.5	0.0037	26.3 ± 4.1	33.6 ± 3.5	0.9605
Total Phenolics (g L^{-1})	1.19 ± 0.04	1.22 ± 0.05	>0.9999	1.23 ± 0.07	1.36 ± 0.07	>0.9999

The harvested fruit was analysed for its chemical composition. Total soluble sugars, pH, and total phenolic content were similar between asymptomatic and SD vines in both seasons. However, fruit from SD vines consistently had a trend towards higher titratable acidity (TA) and total anthocyanin concentration in both seasons.

Differential transcript expression of SD symptomatic vines

In addition to viral identification, the transcriptomic data provided the means to investigate regulatory responses in the host grapevine that were associated with viral infection. Transcript expression profiles were compared across phloem tissue samples collected from SD (n=4) and asymptomatic (n=8) vines. Unsupervised hierarchical clustering of the normalised transcript count matrix revealed two distinctive clusters correlating with the SD and asymptomatic samples (Figure S1) and indicated that these biological replicates were suitable for DE analysis.

In phloem tissues, a total of 1865 differentially expressed (DE) transcripts were identified after filtering (1 < Log2FC < -1 and an adjusted p-value < 0.005) and 1448 and 417 transcripts up and downregulated, respectively (Table S1). To obtain a global overview of the biological processes affected in SD vines, DE transcripts were annotated using GO terms and then subjected to functional enrichment analysis. The upregulated transcripts were classified into eight GO terms and they are primarily involved in phloem development and systemic acquired resistance (SAR) (Figure 2b). For instance, the top upregulated genes were comprised primarily of Sieve Element (SE) Occlusion-like proteins (Figure 2a), which have been linked to SE protein filament formation in eudicotyledons [34-36]. Several biotic stress responsive genes were also significantly upregulated including Expansin 16 (EXPA16), downy mildew resistant 6 (DMR6), WRKY DNA-binding protein 50, defective in induced resistance 1 (DIR1), ribosomal protein S2 (RPS2) and enhanced disease susceptibility 1 (EDS1) (Figure 2a). Downregulated transcripts were enriched in several GO terms linked to stress response, protein assembly and photosynthesis (Figure 2b). DE analysis also revealed that genes encoding DEAD-box ATP-dependent RNA helicase 46 and heat shock proteins (HSP), as well as photosynthesis-associated genes were significantly downregulated in SD-affected phloem samples at the harvesting stage (Figure 2a, b).

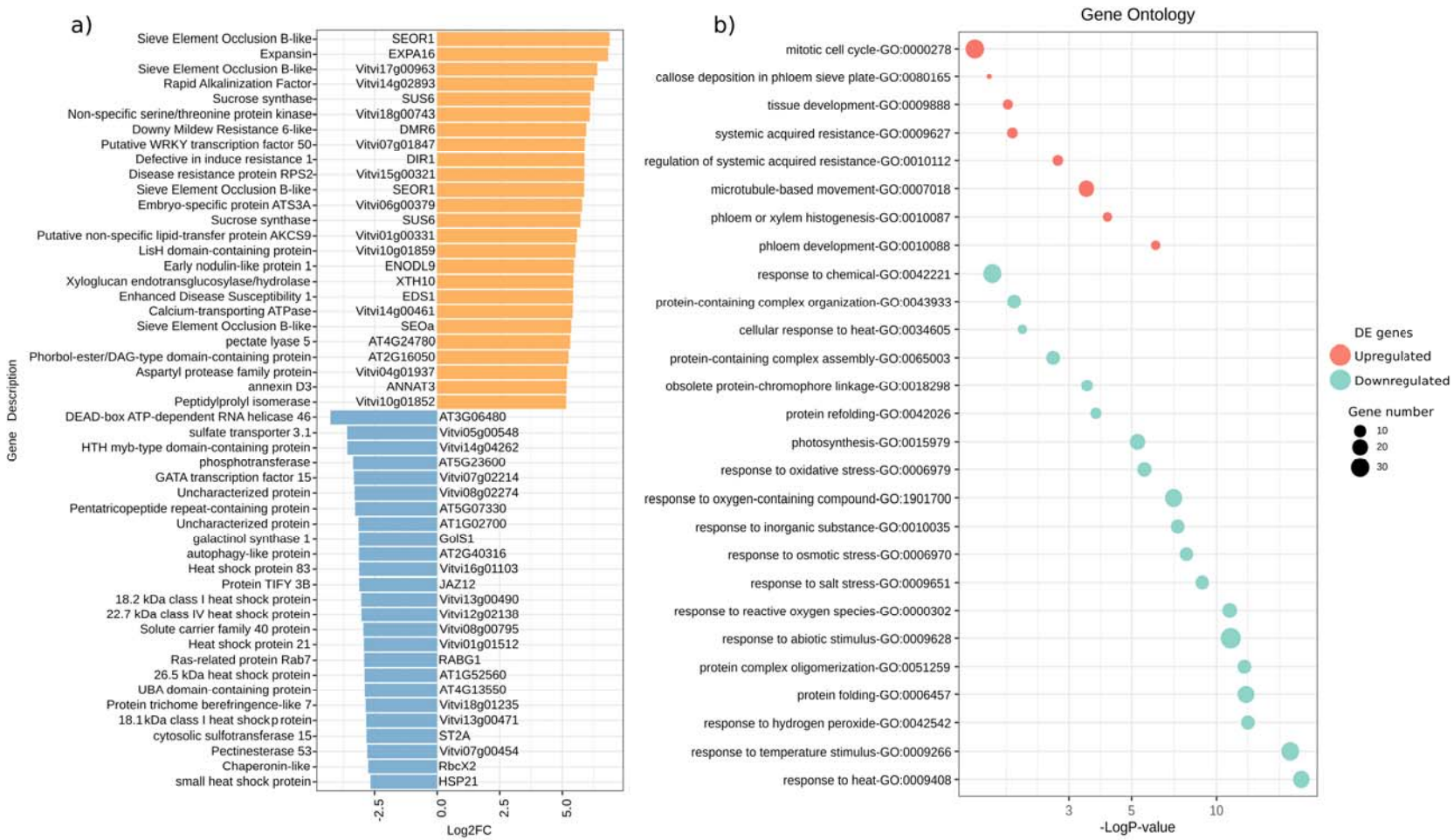

Figure 2. Differential transcript expression analysis between Shiraz Disease (SD) and asymptomatic grapevine samples. a) Top 50 differentially expressed transcripts between SD and asymptomatic samples. Predicted functional annotations (y axis) and gene names relative to orthologues of *Arabidopsis thaliana* are included when available. b) Gene Ontology (GO) enriched terms in the upregulated and downregulated transcript sets.

Discussion

Grapevines and other woody crops affected by viral diseases are often observed to be co-infected with multiple viruses. This co-infection occurs as vectors transmit multiple viruses to the same host. In our study, GVA and GLRaV-4s (strain 9) was predominantly detected in SD vines whereas GRSPaV and GRVFV were detected in both SD-affected and asymptomatic vines. In a mixed infection, in addition to the virus-host-vector interactions, intra-virus and other intra-multipathogenic associations can also play a major role in disease establishment and pathogenicity. Multiple virus infections have been found to cause antagonistic, synergistic or mutually beneficial interactions [37, 38]. A previous study by Rowhani, Daubert [39] has suggested that GLRaVs may have a synergistic interaction with vitiviruses as vines co-infected with GLRaV (GLRaV-1, 2 or 3) and vitiviruses (GVA and GVB) showed significantly higher vitivirus-associated titer, while GLRaV titer remained constant relative to control vines without co-infections. As both GVA and GLRaV-4 strain 9 were consistently detected in all SD-affected vines (Figure 1a), our study further supports the hypothesis that enhanced pathogenicity may have been caused by the synergistic effect induced by these two viral species. Among the three GVA molecular groups, mixed infections of GVA groups II and III were detected in SD vines (Figure 1c). A recent survey of GVA variants in Australian vineyards suggests that GVA group II is the only variant likely to be associated with SD, while GVA variants I and III may not be associated with SD symptoms, at least in Shiraz [40]. The disease symptoms observed in our study therefore likely to be due to the GVA variant II, with symptoms potentially exacerbated by the presence of co-infection by GLRaV.

SD infection causes significant reductions of vine physiological and reproductive performance

Our physiological data indicate a significant reduction of leaf net photosynthesis in SD-affected vines relative to asymptomatic vines (Table 1). This reduction in net photosynthesis can be primarily attributed to a marked reduction of stomatal conductance, photosystem II efficiency, and downregulation of genes associated with photosynthesis. In line with our observations, previous studies have also reported a considerable reduction of photosynthesis, stomatal conductance, PSII efficiency and repression of genes involved in photosystem and photosynthetic pigment biosynthesis in response to GLRaV-3 and phytoplasma [41-44]. Consistent with our observations, grapevines infected with grapevine leafroll disease had similar water status to healthy or uninfected vines [41, 44]. Co-infection of grapevines with both GLRaV-3 and GVA were also found to repress photosynthetic genes and induce defence responsive genes [45].

The significant reductions in carbon and nutrient assimilation observed in the SD-affected vines had a direct influence on reproductive performance as exhibited in reduced yield and bunch numbers relative to asymptomatic vines (Table 2). No differences in berry weight were observed between infected and asymptomatic vines, indicating that carbohydrate accumulation in berries was unaltered within a season. However, in the first season, severely SD-infected vines had a 72% yield reduction (compared to healthy vines), while in the second season a reduction of 83% was observed. This yield loss could be attributed to reduced bunch numbers rather than smaller berries, with the number of bunches per vine likely impacted by cumulative environmental effects as well as vine nutrition. These yield reductions lead to significant economic losses to grape growers and, furthermore, shorten the productive lifespan of diseased vineyards leading to further economic losses associated with roguing (vine removal) and replanting [3].

The physiological and economic impacts of grapevine leafroll viruses have been well documented [46-48]. It has long been known that GLRaV-1 and GLRaV-3, which are the most prevalent and commonly associated with grapevine leafroll disease (GLRD), induce leaf morphological and physiological alterations due to downregulation of carbon assimilation and stomatal conductance, which in turn affect yield and berry composition [41, 49-51]. It has also been reported that total chlorophyll content and total carotenoids are significantly reduced in GLRaV-3 infected red-berried cultivars relative to virus-free leaves [52]. On the contrary, a strain of GLRaV-2 does not impact fruit yield or berry quality [53] and GLRaV-4 has been reported to cause mild GLRD symptoms [47, 54]. We speculate that GLRaV-4 alone may not or only mildly elicit leafroll symptoms, however, when co-existing with GVA, its presence may result in the development of the severe SD symptoms observed in this study.

SD induced changes to berry chemical composition

In order to investigate how SD-induced changes in plant physiology and alter berry chemical composition, which ultimately determines alcohol concentration, wine flavour and aroma, we assessed various chemical parameters in berry juice. Berries from SD-affected vines contained significantly higher TA, total anthocyanin concentration and fruit colour and lower hue relative to asymptomatic vines (Table 2), indicating a modification of carbon allocation and partitioning. A previous study by Mannini, Mollo [53] documented higher TA in grapes from vines with mixed infection of GLRaV-1, GVA and GRSPaV. However, decrease in anthocyanin concentrations have been reported in GLRaV-3 infected vines due to significant downregulation of genes associated with anthocyanin biosynthesis [49, 54]. Anthocyanin accumulation in berries as well as leaves in response to SD infection may play a pivotal role in protecting plants from free radicals. Interestingly, total soluble solids (^{o}Brix), which is an important criterion determining the grape harvest date, was unaffected by SD and may be due to unaltered sugar translocation in the phloem. The pH and total phenol concentration were also unaltered in SD-infected berries. The latter result was consistent with Montero, Mundy [55] who reported no differences in phenol concentration in GLRaV-3-infected vines compared to healthy vines.

SD suppresses vine immunity

A range of genes were shown to be downregulated that are associated with host defence responses and photosynthesis (Figure 2a, b). Particularly, DEAD-box RNA helicase 46 and HSP were repressed in SD-affected phloem tissues at the harvest stage. RNA helicases are ubiquitous enzymes that can dissociate double-stranded RNAs and rearrange RNA secondary structures for regulating vital genetic processes such as replication, transcription and translation [56]. The DEAD-box proteins are the largest helicase subfamily and their vital roles in plant growth and abiotic/biotic stress tolerance have been reported in several plant species such as *Arabidopsis*, grapevine, rice, tomato and sweet potato [57-61]. A total of 40 DEAD-box genes were recently identified in grapevine [61], but their precise functions during pathogen infections remain to be elucidated. Li, Liu [62] demonstrated that ectopic overexpression of rice *BIRH1*, which encodes a DEAD-box RNA helicase, led to enhanced expression of oxidative defence genes and disease resistance to *Alternaria brassicicola* and *Pseudomonas syringae* in *Arabidopsis* [73]. As this evidence supports the putative role of DEAD-box RNA helicases in disease resistance, their downregulation in SD-affected phloem tissues may indicate high disease susceptibility of the symptomatic vines.

Heat shock proteins (HSPs) are ubiquitous cellular components, which regulate cellular homeostasis under both optimal and stress conditions. Their vital roles in protein folding, protein assembly and chaperone functions are well documented [63-65]. A large body of evidence has demonstrated that HSPs play a major role in the development of innate immunity in plants upon pathogen infections. The plant's first mode of defence against pathogen infection includes recognition of pathogen-derived pathogen-associated molecular patterns (PAMPs) and effector proteins by pattern recognition receptors (PRRs) and resistance (R) proteins, respectively [66]. The HSPs contribute to innate immunity via accumulation of PRRs and stabilisation of R proteins [67]. Previous studies have shown that grapevine HSP genes can either be upregulated or downregulated in response to virus infections [42, 68, 69]. Downregulation of *HSPs* expression is suggestive of the suppressed immunity of SD-affected vines.

SD-associated viruses induce systemic acquired resistance

Pathogen infections in plants induce broad-spectrum disease resistance to secondary infections through activating complex systemic acquired resistance (SAR) mechanisms. Our results show that SD-associated viruses primarily upregulate several genes associated with salicylic acid signalling pathway, which plays a major role in inducing SAR [70]. Previous studies have shown that salicylic acid is synthesised at the site of infection and transported to uninfected distal tissues via phloem to establish long-lasting SAR throughout the plant [71]. Salicylic acid enhances the expression of *pathogenesis-related (PR)* genes that encode proteins which directly affect pathogen growth and proliferation [72]. In addition to SAR-associated genes, sieve element occlusion-like genes, calcium transporting ATPase, and genes associated with callose deposition and phloem development were also upregulated in SD-affected phloem tissues (Figure 3a, b). The sieve elements in the phloem are highly specialised conducting cells that have been designed for long-distance transport of photosynthates, plant growth regulators, and defence and stress signalling molecules. Nutrient-rich phloem tissues serve as an ecological niche for a variety of phloem-borne pathogens and insects. Occlusion of phloem sieve plates by callose deposition is a unique and localised defence strategy against phloem-borne viruses to limit their spread in the plant [73]; this occlusion is dependent on free Ca^{2+} accumulation in the sieve plates [74]. Upregulation of calcium transporting ATPase and Expansin 16 (EXPA16) (Figure 2a), which are involved in regulation of cell wall expansion in SD-affected phloem tissues, may be an indication of compromised integrity of sieve tubes. SD-affected vines may therefore be attempting to limit the internal spreading of the SD viruses by blocking phloem sieve elements.

Collectively, the results of our study suggest that vines displaying severe SD symptoms are infected with multiple viruses, including GVA and GLRaV. A recent metagenomic study on SD-associated viruses supports this claim that GVA group II could be the main causal agent of SD [5], which is also supported by these findings. However, similar to our observations, most of the SD-affected grapevines reported in the literature contained at least one GLRaV species (typically GLRaV-3 and/or GLRaV-4) together with GVA, suggesting that this association may be needed to increase virulence [5].

Acknowledgement

We gratefully acknowledge the financial support provided by the University of Adelaide and the Australian Wine Research Institute's Friendship Fund for this research. We also thank Felipe Canela for technical assistance with the field data collection.

References

1. Fuchs, M. Grapevine viruses: A multitude of diverse species with simple but overall poorly adopted management solutions in the vineyard. *Journal of Plant Pathology* 2020, **102,** 643-653.
2. Martelli, G. Infectious diseases and certification of grapevine. *Options Mediterraneennes Serie B* 1997, **29,** 47-64.
3. Wu, Q., N. Habili, F. Constable, et al. Virus pathogens in Australian vineyards with an emphasis on shiraz disease. *Viruses* 2020, **12,** 818.
4. Goszczynski, D. and N. Habili Grapevine virus A variants of group II associated with Shiraz disease in South Africa are present in plants affected by Australian Shiraz disease, and have also been detected in the USA. *Plant Pathology* 2012, **61,** 205-214.
5. Wu, Q., N. Habili, W.M. Kinoti, et al. A metagenomic investigation of the viruses associated with Shiraz Disease in Australia. *Viruses* 2023, **15,** 774.
6. Martelli, G.P. Virus diseases of grapevine. *e LS* 2001,
7. Rosciglione, B., M. Castellano, G. Martelli, et al. Mealybug transmission of grapevine virus A. *Vitis* 1983, **22,** 331-347.
8. Goszczynski, D., J. Du Preez, and J. Burger Molecular divergence of Grapevine virus A (GVA) variants associated with Shiraz disease in South Africa. *Virus Research* 2008, **138,** 105-110.
9. Goszczynski, D. Single□strand conformation polymorphism (SSCP), cloning and sequencing reveal a close association between related molecular variants of Grapevine virus A (GVA) and Shiraz disease in South Africa. *Plant Pathology* 2007, **56,** 755-762.
10. Minafra, A., P. Saldarelli, and G. Martelli Grapevine virus A: nucleotide sequence, genome organization, and relationship in the Trichovirus genus. *Archives of Virology* 1997, **142,** 417-423.
11. Galiakparov, N., E. Tanne, I. Sela, et al. Functional analysis of the grapevine virus A genome. *Virology* 2003, **306,** 42-50.
12. Goszczynski, D. and A. Jooste The application of single-strand conformation polymorphism (SSCP) technique for the analysis of molecular heterogeneity of grapevine virus A. *Vitis* 2002, **41,** 77-82.
13. Goszczynski, D. Complete genome sequence of a natural mutant of grapevine virus A (GVA). *Archives of virology* 2014, **159,** 2523-2528.
14. Goszczynski, D.E. and A. Jooste Identification of divergent variants of Grapevine virus A. *European Journal of Plant Pathology* 2003, **109,** 397-403.
15. Pagay, V. Evaluating a novel microtensiometer for continuous trunk water potential measurements in field-grown irrigated grapevines. *Irrigation Science* 2022, **40,** 45-54.
16. Murchie, E.H. and T. Lawson Chlorophyll fluorescence analysis: a guide to good practice and understanding some new applications. *Journal of experimental botany* 2013, **64,** 3983-3998.
17. Rahimzadeh-Bajgiran, P., B. Tubuxin, and K. Omasa Estimating chlorophyll fluorescence parameters using the joint Fraunhofer line depth and laser-induced saturation pulse (FLD-LISP) method in different plant species. *Remote Sensing* 2017, **9,** 599.
18. Flexas, J., J. Escalona, and H. Medrano Down-regulation of photosynthesis by drought under field conditions in grapevine leaves. *Functional Plant Biology* 1998, **25,** 893-900.
19. Maxwell, K. and G.N. Johnson Chlorophyll fluorescence—a practical guide. *Journal of Experimental Botany* 2000, **51,** 659-668.
20. Galle, A., I. Florez-Sarasa, A. Thameur, et al. Effects of drought stress and subsequent rewatering on photosynthetic and respiratory pathways in Nicotiana sylvestris wild type and

the mitochondrial complex I-deficient CMSII mutant. *Journal of Experimental Botany* 2010, **61,** 765-775.

21. Santi, S., S. Grisan, A. Pierasco, et al. Laser microdissection of grapevine leaf phloem infected by stolbur reveals site specific gene responses associated to sucrose transport and metabolism. *Plant, Cell & Environment* 2013, **36,** 343-355.
22. Liefting, L.W., D.W. Waite, and J.R. Thompson Application of Oxford Nanopore technology to plant virus detection. *Viruses* 2021, **13,** 1424.
23. Deng, Z.-L., P.C. Münch, R. Mreches, et al. Rapid and accurate identification of ribosomal RNA sequences via deep learning. *Nucleic Acids Research* 2022, **50,** e60-e60.
24. Grabherr, M.G., B.J. Haas, M. Yassour, et al. Full-length transcriptome assembly from RNA-Seq data without a reference genome. *Nature Biotechnology* 2011, **29,** 644-652.
25. Langmead, B., M.C. Schatz, J. Lin, et al. Searching for SNPs with cloud computing. *Genome Biology* 2009, **10,** 1-10.
26. Li, B. and C.N. Dewey RSEM: accurate transcript quantification from RNA-Seq data with or without a reference genome. *BMC Bioinformatics* 2011, **12,** 1-16.
27. Katoh, K. and D.M. Standley MAFFT multiple sequence alignment software version 7: improvements in performance and usability. *Molecular Biology and Evolution* 2013, **30,** 772-780.
28. Nguyen, N.-p., S. Mirarab, B. Liu, et al. TIPP: taxonomic identification and phylogenetic profiling. *Bioinformatics* 2014, **30,** 3548-3555.
29. Kalyaanamoorthy, S., B.Q. Minh, T.K. Wong, et al. ModelFinder: fast model selection for accurate phylogenetic estimates. *Nature Methods* 2017, **14,** 587-589.
30. Bray, N.L., H. Pimentel, P. Melsted, et al. Near-optimal probabilistic RNA-seq quantification. *Nature Biotechnology* 2016, **34,** 525-527.
31. Love, M., S. Anders, and W. Huber Differential analysis of count data–the DESeq2 package. *Genome Biology* 2014, **15,** 10-1186.
32. Raudvere, U., L. Kolberg, I. Kuzmin, et al. g: Profiler: a web server for functional enrichment analysis and conversions of gene lists (2019 update). *Nucleic acids research* 2019, **47,** W191-W198.
33. Coetzee, B., M.-J. Freeborough, H.J. Maree, et al. Deep sequencing analysis of viruses infecting grapevines: virome of a vineyard. *Virology* 2010, **400,** 157-163.
34. Anstead, J.A., D.R. Froelich, M. Knoblauch, et al. Arabidopsis P-protein filament formation requires both AtSEOR1 and AtSEOR2. *Plant and Cell Physiology* 2012, **53,** 1033-1042.
35. Jekat, S.B., A.M. Ernst, A.v. Bohl, et al. P-proteins in Arabidopsis are heteromeric structures involved in rapid sieve tube sealing. *Frontiers in Plant Science* 2013, **4,** 225.
36. Musetti, R., S.V. Buxa, F. De Marco, et al. Phytoplasma-triggered Ca2+ influx is involved in sieve-tube blockage. *Molecular Plant-Microbe Interactions* 2013, **26,** 379-386.
37. Syller, J. and A. Grupa Antagonistic within host interactions between plant viruses: molecular basis and impact on viral and host fitness. *Molecular plant pathology* 2016, **17,** 769-782.
38. Mascia, T. and D. Gallitelli Synergies and antagonisms in virus interactions. *Plant Science* 2016, **252,** 176-192.
39. Rowhani, A., S. Daubert, K. Arnold, et al. Synergy between grapevine vitiviruses and grapevine leafroll viruses. *European Journal of Plant Pathology* 2018, **151,** 919-925.
40. Wu, Q., W.M. Kinoti, N. Habili, et al. Genetic diversity of Grapevine Virus A in three Australian vineyards using amplicon high throughput sequencing (Amplicon-HTS). *Viruses* 2024, **16,** 42.
41. Endeshaw, S.T., P. Sabbatini, G. Romanazzi, et al. Effects of grapevine leafroll associated virus 3 infection on growth, leaf gas exchange, yield and basic fruit chemistry of *Vitis vinifera* L. cv. Cabernet Franc. *Scientia Horticulturae* 2014, **170,** 228-236.
42. Espinoza, C., A. Vega, C. Medina, et al. Gene expression associated with compatible viral diseases in grapevine cultivars. *Functional & Integrative Genomics* 2007, **7,** 95-110.
43. Hren, M., P. Nikolić, A. Rotter, et al. 'Bois noir'phytoplasma induces significant reprogramming of the leaf transcriptome in the field grown grapevine. *BMC Genomics* 2009, **10,** 1-17.

44. Moutinho□Pereira, J., C. Correia, B. Gonçalves, et al. Impacts of leafroll□associated viruses (GLRaV□1 and□3) on the physiology of the P ortuguese grapevine cultivar 'T ouriga N acional'growing under field conditions. *Annals of Applied Biology* 2012, **160,** 237-249.
45. Punelli, F., M. Al Hassan, V. Fileccia, et al. A microarray analysis highlights the role of tetrapyrrole pathways in grapevine responses to "stolbur" phytoplasma, phloem virus infections and recovered status. *Physiological and Molecular Plant Pathology* 2016, **93,** 129-137.
46. Atallah, S.S., M.I. Gómez, M.F. Fuchs, et al. Economic impact of grapevine leafroll disease on Vitis vinifera cv. Cabernet franc in Finger Lakes vineyards of New York. *American Journal of Enology and Viticulture* 2012, **63,** 73-79.
47. Song, Y., R.H. Hanner, and B. Meng Probing into the effects of grapevine leafroll-associated viruses on the physiology, fruit quality and gene expression of grapes. *Viruses* 2021, **13,** 593.
48. Halldorson, M.M. and M. Keller Grapevine leafroll disease alters leaf physiology but has little effect on plant cold hardiness. *Planta* 2018, **248,** 1201-1211.
49. Alabi, O.J., L.F. Casassa, L.R. Gutha, et al. Impacts of grapevine leafroll disease on fruit yield and grape and wine chemistry in a wine grape (*Vitis vinifera* L.) cultivar. *PLoS One* 2016, **11,** e0149666.
50. Guidoni, S., A. Ferrandino, and V. Novello Effects of seasonal and agronomical practices on skin anthocyanin profile of Nebbiolo grapes. *American Journal of Enology and Viticulture* 2008, **59,** 22-29.
51. Kovacs, L.G., H. Hanami, M. Fortenberry, et al. Latent infection by leafroll agent GLRaV-3 is linked to lower fruit quality in French-American hybrid grapevines Vidal blanc and St. Vincent. *American Journal of Enology and Viticulture* 2001, **52,** 254-259.
52. Gutha, L.R., L.F. Casassa, J.F. Harbertson, et al. Modulation of flavonoid biosynthetic pathway genes and anthocyanins due to virus infection in grapevine (*Vitis vinifera* L.) leaves. *BMC Plant Biology* 2010, **10,** 1-18.
53. Mannini, F., A. Mollo, and R. Credi Field performance and wine quality modification in a clone of Vitis vinifera cv. Dolcetto after GLRaV-3 elimination. *American Journal of Enology and Viticulture* 2012, **63,** 144-147.
54. Naidu, R.A., H.J. Maree, and J.T. Burger Grapevine leafroll disease and associated viruses: a unique pathosystem. *Annual Review of Phytopathology* 2015, **53,** 613-634.
55. Montero, R., D. Mundy, A. Albright, et al. Effects of Grapevine Leafroll associated Virus 3 (GLRaV-3) and duration of infection on fruit composition and wine chemical profile of *Vitis vinifera* L. cv. Sauvignon blanc. *Food Chemistry* 2016, **197,** 1177-1183.
56. de la Cruz, J., D. Kressler, and P. Linder Unwinding RNA in *Saccharomyces cerevisiae*: DEAD-box proteins and related families. *Trends in Biochemical Sciences* 1999, **24,** 192-198.
57. Jarmoskaite, I. and R. Russell RNA helicase proteins as chaperones and remodelers. *Annual Review of Biochemistry* 2014, **83,** 697-725.
58. Yarra, R. and Y. Xue Ectopic expression of nucleolar DEAD-Box RNA helicase OsTOGR1 confers improved heat stress tolerance in transgenic Chinese cabbage. *Plant Cell Reports* 2020, **39,** 1803-1814.
59. Cai, J., X. Meng, G. Li, et al. Identification, expression analysis, and function evaluation of 42 tomato DEAD-box RNA helicase genes in growth development and stress response. *Acta Physiologiae Plantarum* 2018, **40,** 1-11.
60. Wan, R., J. Liu, Z. Yang, et al. Genome-wide identification, characterisation and expression profile analysis of DEAD-box family genes in sweet potato wild ancestor *Ipomoea trifida* under abiotic stresses. *Genes & Genomics* 2020, **42,** 325-335.
61. YANG, S.-d., D.-l. GUO, M.-s. PEI, et al. Identification of the DEAD-box RNA helicase family members in grapevine reveals that *VviDEADRH25a* confers tolerance to drought stress. *Journal of Integrative Agriculture* 2022, **21,** 1357-1374.
62. Li, D., H. Liu, H. Zhang, et al. OsBIRH1, a DEAD-box RNA helicase with functions in modulating defence responses against pathogen infection and oxidative stress. *Journal of Experimental Botany* 2008, **59,** 2133-2146.
63. Whitley, D., S.P. Goldberg, and W.D. Jordan Heat shock proteins: a review of the molecular chaperones. *Journal of Vascular Surgery* 1999, **29,** 748-751.

64. Wang, W., B. Vinocur, O. Shoseyov, et al. Role of plant heat-shock proteins and molecular chaperones in the abiotic stress response. *Trends in Plant Science* 2004, **9,** 244-252.
65. Hafrén, A., D. Hofius, G. Rönnholm, et al. HSP70 and its cochaperone CPIP promote potyvirus infection in *Nicotiana benthamiana* by regulating viral coat protein functions. *The Plant Cell* 2010, **22,** 523-535.
66. Chisholm, S.T., G. Coaker, B. Day, et al. Host-microbe interactions: shaping the evolution of the plant immune response. *Cell* 2006, **124,** 803-814.
67. Hubert, D.A., P. Tornero, Y. Belkhadir, et al. Cytosolic HSP90 associates with and modulates the Arabidopsis RPM1 disease resistance protein. *The EMBO journal* 2003, **22,** 5679-5689.
68. Gambino, G., D. Cuozzo, M. Fasoli, et al. Co-evolution between Grapevine rupestris stem pitting-associated virus and *Vitis vinifera* L. leads to decreased defence responses and increased transcription of genes related to photosynthesis. *Journal of Experimental Botany* 2012, **63,** 5919-5933.
69. Zhang, L., D. Fan, H. Li, et al. Characterization and identification of grapevine heat stress-responsive microRNAs revealed the positive regulated function of vvi-miR167 in thermostability. *Plant Science* 2023, **329,** 111623.
70. Gaffney, T., L. Friedrich, B. Vernooij, et al. Requirement of salicylic acid for the induction of systemic acquired resistance. *Science* 1993, **261,** 754-756.
71. Shulaev, V., J. León, and I. Raskin Is salicylic acid a translocated signal of systemic acquired resistance in tobacco? *The Plant Cell* 1995, **7,** 1691-1701.
72. Zhang, J., X. Du, Q. Wang, et al. Expression of pathogenesis related genes in response to salicylic acid, methyl jasmonate and 1-aminocyclopropane-1-carboxylic acid in *Malus hupehensis* (Pamp.) Rehd. *BMC Research Notes* 2010, **3,** 1-6.
73. Hao, P., C. Liu, Y. Wang, et al. Herbivore-induced callose deposition on the sieve plates of rice: an important mechanism for host resistance. *Plant Physiology* 2008, **146,** 1810-1820.
74. Jiang, Y., C.-X. Zhang, R. Chen, et al. Challenging battles of plants with phloem-feeding insects and prokaryotic pathogens. *Proceedings of the National Academy of Sciences* 2019, **116,** 23390-23397.